

RESEARCH PAPER



The autoimmune susceptibility gene, *PTPN2*, restricts expansion of a novel mouse adherent-invasive *E. coli*

Ali Shawki ^a, Rocio Ramirez^{a*}, Marianne R. Spalinger^a, Paul M. Ruegger^b, Anica Sayoc-Becerra^a, Alina N. Santos ^a, Pritha Chatterjee^a, Vinicius Canale ^a, Jonathan D. Mitchell^b, John C. Macbeth^b, Casey M. Gries^a, Michel L. Tremblay ^c, Ansel Hsiao^b, James Borneman^b, and Declan F. McCole ^a

^aDivision of Biomedical Sciences, University of California Riverside, Riverside, California, USA; ^bDepartment of Microbiology and Plant Pathology, University of California Riverside, Riverside, California, USA; ^cDepartment of Biochemistry, McGill University, Montreal, Quebec, Canada

ABSTRACT

Inflammatory bowel disease (IBD) pathogenesis involves significant contributions from genetic and environmental factors. Loss-of-function single-nucleotide polymorphisms (SNPs) in the protein tyrosine phosphatase non-receptor type 2 (*PTPN2*) gene increase IBD risk and are associated with altered microbiome population dynamics in IBD. Expansion of intestinal pathobionts, such as adherent-invasive *E. coli* (AIEC), is strongly implicated in IBD pathogenesis as AIEC increases pro-inflammatory cytokine production and alters tight junction protein regulation – suggesting a potential mechanism of pathogen-induced barrier dysfunction and inflammation. We aimed to determine if *PTPN2* deficiency alters intestinal microbiome composition to promote expansion of specific bacteria with pathogenic properties. In mice constitutively lacking *Ptpn2*, we identified increased abundance of a novel mouse AIEC (*mAIEC*) that showed similar adherence and invasion of intestinal epithelial cells, but greater survival in macrophages, to the IBD-associated AIEC, LF82. Furthermore, *mAIEC* caused disease when administered to mice lacking segmented-filamentous bacteria (SFB), and in germ-free mice but only when reconstituted with a microbiome, thus supporting its classification as a pathobiont, not a pathogen. Moreover, *mAIEC* infection increased the severity of, and prevented recovery from, induced colitis. Although *mAIEC* genome sequence analysis showed >90% similarity to LF82, *mAIEC* contained putative virulence genes with >50% difference in gene/protein identities from LF82 indicating potentially distinct genetic features of *mAIEC*. We show for the first time that an IBD susceptibility gene, *PTPN2*, modulates the gut microbiome to protect against a novel pathobiont. This study generates new insights into gene-environment-microbiome interactions in IBD and identifies a new model to study AIEC-host interactions.

ARTICLE HISTORY

Received 28 February 2020
Revised 30 April 2020
Accepted 18 May 2020

KEYWORDS

AIEC; Caco-2; colitis; epithelial; inflammatory bowel disease; LF82; macrophage; microbiome

Introduction

Genome-wide association studies (GWAS) have identified an association between loss-of-function single-nucleotide polymorphisms (SNPs) in the protein tyrosine phosphatase non-receptor type 2 (*PTPN2*) gene, that encodes the T-cell protein tyrosine phosphatase (TCPTP), and several autoimmune diseases including Crohn's disease, ulcerative colitis, celiac disease, type 1 diabetes and rheumatoid arthritis.^{1–5} Crohn's disease (CD) and ulcerative colitis (UC), collectively known as inflammatory bowel disease (IBD), are chronic intestinal inflammatory conditions whose etiology

is unclear. Several factors such as genetics and alterations in the intestinal microbiome are critical determinants of IBD pathogenesis.⁶ TCPTP has an essential role in restricting inflammation as homozygous *Ptpn2* knockout mice exhibit substantially increased expression of pro-inflammatory cytokines and uncontrolled systemic inflammation.^{7,8} TCPTP regulation of inflammation is due, at least in part, to restriction of pro-inflammatory signaling pathways mediated by members of the Janus kinases (JAKs) and signal transducer and activator of transcription (STAT) families of signaling molecules (JAK-STATs).

CONTACT Declan F. McCole  declan.mccole@ucr.edu  Division of Biomedical Sciences, School of Medicine, University of California Riverside, Riverside, CA 92521; James Borneman borneman@ucr.edu Department of Microbiology and Plant Pathology, University of California Riverside, 3401 Watkins Drive, Multidisciplinary Research Building Room 4130, Riverside, CA 92521

*Current address: Biomedical Sciences, Cedars-Sinai Medical Center, Los Angeles, California, USA.

 Supplemental data for this article can be accessed [here](#).

JAK-STAT signaling can be activated by inflammatory cytokines such as interferon-gamma (IFN- γ) that is involved in several autoimmune diseases including IBD and celiac disease.^{8,9} TCPTP can restrict intestinal epithelial cell (IEC) barrier defects and tight junction remodeling induced by IFN- γ .⁸⁻¹¹ The intestinal epithelium forms a selectively permeable barrier between the lumen and the submucosa through the formation of multiprotein complexes of desmosomes, adherens junctions and tight junctions (TJ) that regulate paracellular permeability.^{12,13} The intestinal epithelial barrier is essential to maintain appropriate compartmentalization of tissue versus luminal factors in the gut. Specifically, the epithelium ensures that luminal microbes and their products are restricted from accessing lamina propria immune cells or gaining access to the underlying vasculature. Indeed, when intestinal epithelial integrity is compromised, translocation of bacteria and bacterial products such as lipopolysaccharide can occur and trigger inflammatory responses that in severe cases lead to sepsis.¹⁴⁻¹⁶

Approximately 10^{12} – 10^{13} bacteria exist in the adult human gastrointestinal tract with more than 35,000 bacterial species that play a major role in maintaining intestinal homeostasis.¹⁷⁻¹⁹ Alterations in the intestinal microbiome are a major environmental factor in the pathogenesis of IBD.²⁰⁻²² Expansion of pathobionts, such as adherent-invasive *Escherichia coli* (AIEC), is associated with IBD pathogenesis. This is likely due to a combination of pathological activities of AIEC which include induction of pro-inflammatory cytokine (IFN- γ , tumor necrosis factor alpha [TNF- α], interleukin 13 [IL-13]) production; increasing susceptibility to intestinal inflammation in genetically susceptible hosts; and disrupting expression and distribution of epithelial TJ proteins leading to increased intestinal permeability.²³⁻³¹

A major gap in our understanding of how complex inflammatory diseases such as IBD arise, relates to how genetic susceptibility alters the intestinal environment to favor the expansion of commensal microbes with pathogenic potential (i.e., pathobionts) prior to the manifestation of clinical disease.³² Clinical genetic studies have provided some clues in this regard. A role for *PTPN2* as a clinically relevant modulator of the

gut microbiome was first identified in IBD patients where *PTPN2* SNPs influenced the population dynamics of intestinal microbes, while a separate study also identified dysbiosis and increased disease severity in patients harboring *PTPN2* SNPs.^{33,34} 16S ribosomal RNA (rRNA) gene analysis showed that *Ptpn2* deficiency in mouse CD4 T-lymphocytes aggravated adoptive T-cell transfer colitis and promoted a broad dysbiosis featuring typical colitis-associated increases in *Bacteroidetes* and *Proteobacteria*, and decreased *Firmicutes*, in stool samples.³⁵ In this study we aimed to use a more rigorous approach of sequencing the internal transcribed spacer (ITS) variable region of bacteria to (i) identify if constitutive *Ptpn2* loss alters intestinal microbiome composition; and (ii) identify specific bacterial species modulated by *Ptpn2*.³⁶

Here, we report that *Ptpn2*-deficient mice exhibit a highly significant increase in abundance of a novel mouse adherent-invasive *E. coli* that has significant, but also distinct, genetic overlap with the human LF82 originally isolated from a Crohn's disease patient.³⁷ This mouse AIEC (*mAIEC*) caused weight loss in mice housed in specific pathogen-free (SPF) conditions and lacking segmented-filamentous bacteria (SFB-free), and in germ-free mice reconstituted with a microbiome, thus supporting its classification as a pathobiont rather than a pathogen. Furthermore, *mAIEC* exacerbated and delayed recovery from dextran sulfate sodium (DSS) colitis in SPF-SFB-free mice, thus confirming its pathogenic properties. Our data identify a novel mouse AIEC that may prove to be a valuable tool for the study of pathobiont-induced disease and for the interactions of genetic and environmental factors contributing to autoimmune diseases such as IBD.

Methods

Animal procedures

Ethical Statement on Mouse Studies – All animal care and procedures were performed in accordance with institutional guidelines and approved by the University of California, Riverside Institutional Animal Care and Use Committee under Protocol #A20190032E.

Housing and husbandry of experimental animals

– Constitutive *Ptpn2* knockout (KO) male and female mice were generated by breeding of heterozygous (Het) mice on a BALB/c background and genotyped as previously described.⁷ Wild-type (WT) and *Ptpn2*-Het littermate male and female mice were used as controls. All mice used for microbiome analysis were approximately 3 weeks old (19–23 d of age) at time of sacrifice and were housed in specific pathogen-free (SPF) conditions at the University of California, Riverside.

Wild-type 10-week old confirmed SFB-free C57Bl/6 female mice were purchased from JAX labs (Stock# 000664) and housed in SPF conditions.

Germ-free ~12-week old C57Bl/6 male and female mice were generated from within the germ-free facility at the University of California, Riverside.

Microbiome studies

– Lumenal contents (distal ileum, cecum, proximal and distal colon) and mucosal-associated microbes (small and large intestine) were isolated as previously published.³⁸ Intestinal epithelial cells (IEC) were isolated from small and large intestines using the dithiothreitol (DTT)-based (ThermoFisher Scientific, Waltham, MA) intraepithelial lymphocyte release method and the Percoll-based (GE Healthcare Bio-Sciences, Pittsburg, PA) density gradient purification method as previously described.^{39,40} DNA was isolated from the samples using the DNeasy PowerSoil Kit (Qiagen, Germantown, MD) and a 30-s bead-beating step using a Mini-Beadbeater-16 (BioSpec Products, Bartlesville, OK, USA). Illumina bacterial rRNA internal transcribed spacer (ITS) region libraries were constructed as previously described.^{36,41} DNA sequencing (single-end 250 base) was performed using an Illumina MiSeq (Illumina Inc., San Diego, CA).

Bacterial rRNA ITS data processing

– The UPARSE pipeline was used for demultiplexing, length trimming, quality filtering and operational taxonomic unit (OTU) picking using default parameters or recommended guidelines as initially described and which have been updated at https://www.drive5.com/usearch/manual/uparse_pipeline.html.⁴² Briefly, after demultiplexing and using the recommended 1.0 expected error

threshold, sequences were trimmed to a uniform length of 245bp, which kept 65.1% of reads. De-replicated sequences were subjected to error-correction (denoised) and chimera filtering to generate zero-radius operational taxonomic units (ZOTUs) using UNOISE3.⁴³ An OTU table was then generated using the otutab command. ZOTUs having non-bacterial DNA were identified by performing a local BLAST search of their seed sequences against the nucleotide database.⁴⁴ ZOTUs were removed if any of their highest scoring BLAST hits contained taxonomic IDs within the Rodent family, Fungal or Viridiplantae kingdoms, or PhiX. Taxonomic assignments to bacterial ZOTUs were made by finding the lowest common taxonomic level of the highest BLAST hits excluding unclassified designations. The bacterial rRNA ITS sequences have been deposited in the National Center for Biotechnology Information (NCBI) Sequence Read Archive (SRA) under the SRA BioProject Accession Number PRJNA609140.

Bacterial rRNA ITS data analysis

– QIIME was used to calculate Hellinger beta diversity distance matrices, which were depicted using principle coordinates analysis (PCoA), and statistically assessed by performing Adonis tests.^{45,46} Statistical differences among the phylotypes were determined using edgeR and the false discovery rate (FDR) method.^{47–49} Prism (GraphPad, La Jolla, CA) was used to create taxonomic plots.

Isolating the *E. coli* phylotype bacterium (*mAIEC*)

– The mouse AIEC (*mAIEC*) used in this study was isolated using standard microbiological procedures. Briefly, *mAIEC* was isolated from distal colon luminal contents – a region where a significant increase in relative abundance of *mAIEC* was found (see [Figure 3\(a\)](#)) – from a constitutive *Ptpn2*-knockout (KO) mouse using BBA plates – Brucella Agar (BD, Franklin Lakes, NJ) + 5% defibrinated sheep blood (Colorado Serum Company, Denver, CO) – and incubated aerobically at 37°C overnight. We performed a three-step procedure to identify and purify the *mAIEC*. First, *Escherichia coli* colonies were tentatively identified using the PCR-based, Ribosomal Intergenic Spacer Analysis (RISA) method and small portions of individual colonies from the BBA plates as the templates, and the PCR

primers: 1507 F, GGTGAAGTCGTAACAAGGTA and 23SR, GGGTTBCCCCATTCRG (see Suppl. Figure 3 for additional information on this method and PCR amplicon results).⁵⁰ Second, colonies with an *E. coli* banding pattern from the RISA were purified by performing two successive streak-plating procedures to obtain single colonies. The resulting colonies were grown overnight in LB broth, and stored in aliquots in Brucella Broth + 20% glycerol at -80°C . Finally, the strain used in this study – *mAIEC* strain UCR-PP2 – was confirmed to have the identical rRNA ITS nucleotide sequence as the *E. coli* phylotype identified by the Illumina sequence analysis by (i) PCR amplifying the rRNA ITS region of individual colonies using the RISA primers described above, and (ii) using the Sanger method to obtain the nucleotide sequence of the PCR amplicons.³⁶

Bacterial constructs

– To generate a constitutive red fluorescent *mAIEC* (*mAIEC^{red}*), pKB985 which encodes for mCherry was transformed into chemically competent *mAIEC*.^{51,52} Plasmid maintenance was achieved during subculture using chloramphenicol (20 $\mu\text{g}/\text{mL}$) (Sigma-Aldrich, St. Louis, MO).

Bacterial infection studies

– Bacteria from stocks frozen at -80°C in 1:1 vol/vol glycerol:LB were cultured overnight in Luria-Bertani (LB) broth at 37°C , 250–300rpm, and regrown the next day in fresh LB to exponential phase growth. Culture was pelleted, washed with phosphate buffered saline (PBS), and resuspended in PBS. The bacteria used were the LF82 human AIEC (kindly provided by the late Dr. Arlette Darfeuille-Michaud), *mAIEC*, and K12 (a noninvasive *E. coli*, ATCC 25404). Caco-2 brush border (Caco-2BBE) cells were seeded at 2×10^5 cells per well in 24-well plates, cultured until confluent, and infected at a multiplicity of infection (MOI) of 10 bacteria/cell as previously described.^{53,54} Media was changed to antibiotic and serum-free media 24 h prior to infection. For adherence and invasion studies, Caco-2BBE cells were infected with bacteria for 3 h followed by 1 h with fresh media with 100 $\mu\text{g}/\text{mL}$ Gentamicin (Sigma Aldrich, St. Louis, MO) for invasion studies. Bacterial survival was performed using murine J774 macrophages (M ϕ)

(seeded similarly as Caco-2BBE cells above) (ATCC) infected with bacteria at a MOI of 20 for 2 h followed by a PBS wash, incubation with fresh media containing 100 $\mu\text{g}/\text{mL}$ Gentamicin for 1 h followed by incubation with fresh media containing 20 $\mu\text{g}/\text{mL}$ Gentamicin for 24 h. After bacterial infection, cells were washed with PBS and lysed with 1% Triton-X for 5 min. Lysates were plated onto Luria Bertani agar plates and cultured overnight at 37°C .

For imaging of *mAIEC^{red}* in epithelial cells by immunofluorescence, Caco-2BBE cells were seeded at 5×10^5 cells per round coverslip, cultured until 70% confluent, and infected with *mAIEC^{red}* following the invasion studies described above. Cells were washed with PBS (x3) followed by fixation with 4% paraformaldehyde for 20 min at room temperature. Cells were then permeabilized with 0.3% Triton X-100 (ThermoFisher Scientific, Waltham, MA) for 5 min followed by blocking with 5% Bovine Serum Albumin (BSA) for 10 min at room temperature. Cells were incubated with Alexa Fluor 488-Phalloidin antibody (1:1000) (abcam, Cambridge, United Kingdom) for 90 min at room temperature following by nuclei staining with 4,6-diamididino-2-phenylindole (DAPI) (Invitrogen, Carlsbad, CA). Confocal analysis was performed using a CSU-X-1 spinning-disk confocal imager (Yokogawa, Japan) attached to a Zeiss 130 Axio Observer inverted microscope. Hardware was controlled by Micro-Manager imaging software. Phalloidin was visualized using a 488 nm excitation laser and FITC filter set. DAPI was visualized using a 405 nm excitation laser and DAPI filter set. mCherry was visualized using a 561 nm excitation laser and mCherry filter set. Images were analyzed using ImageJ software.

Mice were infected by oral gavage with 10^6 colony forming units (CFU)/mL of *mAIEC^{red}*, or 10^9 CFU/mL of *mAIEC*, or K12 in 100 μL PBS/mouse. Body weight was monitored daily. Colonization and bacterial burden were measured by overnight culture of homogenized samples suspended in 500 μL of PBS.

Induction and assessment of colitis severity and histological score

– Colitis was induced by supplementation of drinking water with dextran-sodium sulfate (DSS) (molecular weight 36,000–50,000) (MP Biomedicals,

Irvine, CA) at 3% for 7 d as described.⁵⁵ Mice were randomized to three groups: 1) H₂O group did not receive DSS but received daily single gavages of PBS (H₂O-PBS) or bacteria (H₂O-K12, H₂O-*m*AIEC) for the first four consecutive days (dosing previously determined, unpublished data (Spalinger et al.)); 2) acute DSS group received DSS for 7 d with daily single gavages of PBS (DSS-PBS) or bacteria (DSS-K12, DSS-*m*AIEC) for the first four consecutive days of DSS treatment followed by 4 d of recovery post DSS treatment; and 3) recovery from colitis group received DSS for 7 d with daily single gavages of PBS (rec-PBS) or bacteria (rec-K12, rec-*m*AIEC) for four consecutive days post DSS treatment.

To assess disease severity of colitis in animals, disease activity index (DAI) was monitored daily as follows: Appearance (0 = smooth, shiny fur; 1 = dull coat, 2 = dull, ruffled fur), Activity (0 = normal, active, 1 = reduced activity, moves when cage is opened, 2 = reluctant to move when touched), Interest (0 = active interest, 1 = reduced interest when cage is opened, 2 = self-isolation, does not interact), Weight (0 = weight gain or no change, 0.5 = weight loss up to 3%, 1 = weight loss up to 5%, 1.5 = weight loss up to 7%, 2 = weight loss over 7%), and Stool consistency (0 = solid, 1 = soft, 2 = very soft but in shape, 3 = liquid) for a total score range of 0–11.^{56,57} Myeloperoxidase, an indicator of infiltration/activation of neutrophilic granulocytes was measured as previously described.^{57,58} Histological scoring for inflammatory infiltration and epithelial cell damage was performed on H&E-stained sections of the most distal 1 cm of the mouse colon.^{35,56,57}

Briefly, sections from the most distal 1 cm of the mouse colon were deparaffinized in Citrisolv and rehydrated using a series of alcohol washes with decreasing concentration, before staining with Hematoxylin for 10 min. The sections were then rinsed with tap water for 10 mins and stained in Eosin Y solution for 15 sec, briefly rinsed in tap water and dehydrated in ethanol with ascending concentrations followed by Citrisolv, and finally mounted with Permout (ThermoFisher Scientific, Waltham, MA). Microscopic assessment was performed using a Leica DM5500 microscope attached to a DFC365 FX camera using a 63× oil immersion objective with an additional 2× digital zoom. The

individual images were converted to tiff files with the LAS-V4.12 lite software, and Photoshop (Adobe) was used to create the final figures (Suppl. Figure 2).

In-vivo barrier permeability

– Mice were gavaged with 80 mg/mL of fluorescein isothiocyanate (FITC)-dextran (4 kDa) (FD4) and 20 mg/mL of rhodamine B-dextran (70 kDa) (RD70). After 5 h, blood was collected by tail bleed (germ-free mice) or retro-orbital bleed into serum collection tubes. Blood was centrifuged at 4° C, 1,500 g, for 15 min, and serum analyzed for FITC-dextran and rhodamine B-dextran concentration with the Veritas Microplate luminometer (Turner Biosystems, Sunnyvale, CA), GloMax software (Promega, Madison, WI), using excitation/emission wavelengths of 490/510–570 nm and 525/580–640 nm, respectively.^{59,60} Standard curves for calculating fluorophore concentration in the samples were obtained by diluting the fluorophore stock in water.

Escherichia coli genome sequencing, assembly, annotation and analysis

– Genome sequences of our *m*AIEC (strain UCR-PP2) and *E. coli* K12 (ATCC 25404) were obtained using shotgun DNA sequencing (Novogene, Sacramento, CA). Genomes were assembled using Spades 3.11.1 and annotated using Prokka 1.13.3.^{61,62} The genome of *m*AIEC was compared with the genome sequence of the human LF82 isolate.³⁷ Putative virulence genes found in *E. coli*'s and other AIECs including LF82 were identified by comparing the known sequence of each gene from K12. Putative virulence genes common between *m*AIEC; another opportunistic mouse *E. coli* with some AIEC features, NC101; and the human LF82 AIEC; or genes unique to each isolate, were compared and the percent identity of each gene and predicted protein between the isolates was determined using EMBOSS Water.^{63,64}

Statistical analyses

– We set critical significance level $\alpha = 0.05$ and analyzed our data using parametric statistics. Data are expressed as mean \pm SD for *n* independent observations per group unless stated otherwise.

Between-group inferences were made by using 1-way or 2-way analysis of variance (ANOVA) and controlled by the false discovery rate (FDR) procedure where applicable.⁶⁵

Results

Constitutive *PTPN2*-deficient mice have an altered intestinal microbiome and expansion of proteobacteria

Since *PTPN2* genotyped human IBD patients show altered intestinal microbiomes, we analyzed the microbiomes of constitutive *Ptpn2*-deficient mice.³⁴ At the community level, analysis of the bacterial rRNA ITS region revealed three distinct regional groups (Figure 1(a)) (Adonis tests, $P = 0.001$). One group was samples from the lumen of the large intestine, comprised of the cecum, proximal colon and distal colon. Another group contained the intestinal epithelial cell (IEC) samples from the small and large intestine, while the third group was samples from the ileal lumen.

An examination of these three regional groups by *Ptpn2* genotype showed that constitutive *Ptpn2*-knockout (KO) mice had different bacterial communities in the lumen of the large intestine

compared with heterozygous (Het) and wild-type (WT) mice (Adonis tests, $P < 0.030$) (Figure 1(b)). In the group comprised of the IECs from the small and large intestine, the communities in *Ptpn2*-KO mice were different than those in the WT mice (Adonis tests, $P = 0.022$) (Figure 1(c)). An analysis of the bacterial communities in the mesenteric lymph nodes and spleen showed that bacterial composition in *Ptpn2*-KO mice was different than in WT mice ($P = 0.005$) (Suppl. Figure 1).

To further investigate the taxa in these regional groups, phyla and species plots were constructed (Figure 2). The most abundant gut bacterial phyla have been reported to be *Bacteroidetes*, *Firmicutes* and *Actinobacteria*.⁶⁶ In our study, the most abundant phylum in the lumen of the large intestine was the *Bacteroidetes* (Figure 2(a)). However, the most abundant phylum in the IECs of the small and large intestine was the *Proteobacteria* (Figure 2(c)). We posit that this difference is caused by the distinct environmental conditions associated with the IECs and the lumen of the gut.

An analysis of the taxa by *Ptpn2* genotype showed more *Proteobacteria* in *Ptpn2*-KO mice than in the WT and Het mice in samples from the lumen of the large intestine and small and

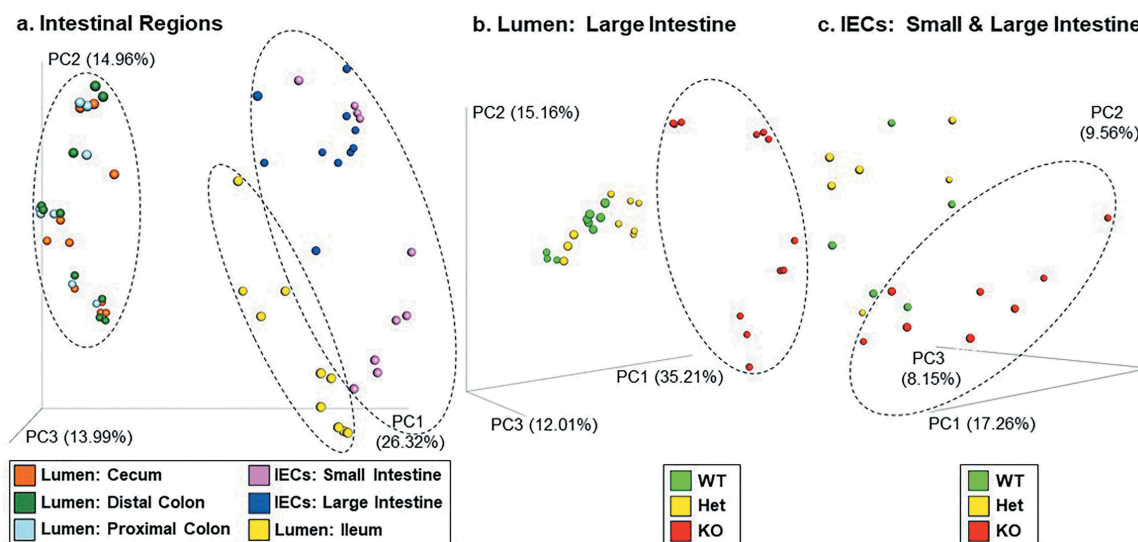


Figure 1. Bacterial Community Analysis by Region and *Ptpn2* Genotype. Beta diversity distance values were generated from bacterial rRNA ITS sequences and displayed using principal-coordinates analysis (PCoA). Adonis tests determined that (a) the three regional groups in the ellipses were different ($P = 0.001$; $n = 18-24$), (b) KO was different than WT and Het ($P < 0.03$; $n = 9-12$) in the lumen of the large intestine (cecum, proximal and distal colon), and (c) KO was different than WT ($P = 0.022$; $n = 6-8$) in the intestinal epithelial cells (IECs) from the small and large intestine.

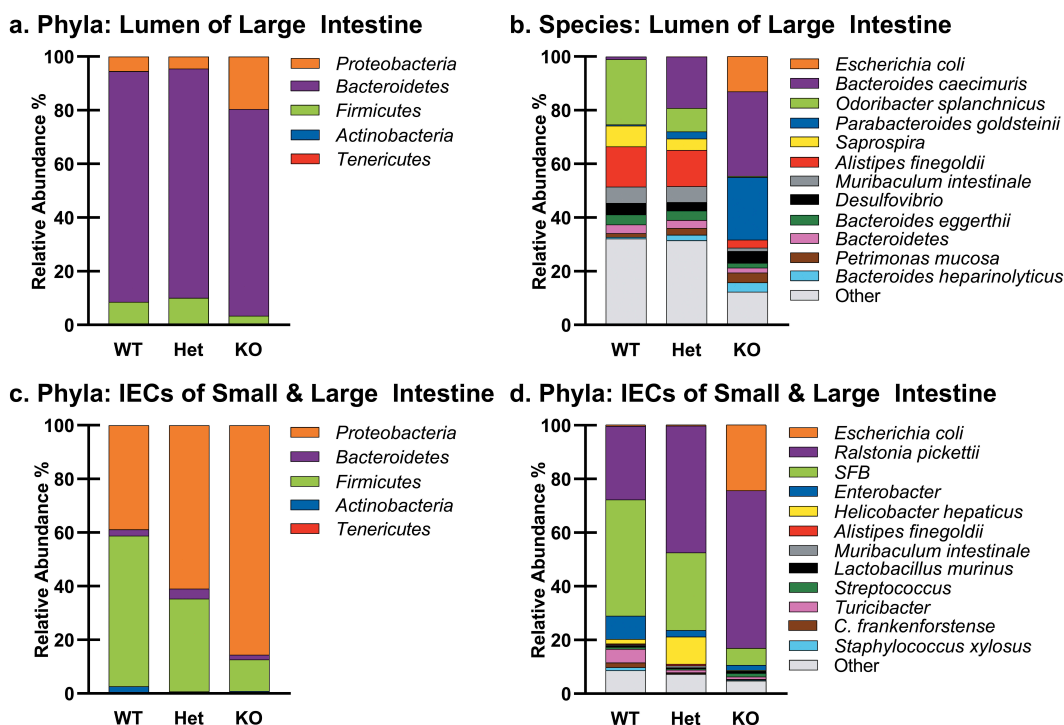


Figure 2. Bacterial Taxa by Region and *Ptpn2* Genotype. Bacterial phyla and species plots of (a,b) the lumen of the large intestine ($n = 9-12$), and (c,d) intestinal epithelial cells (IECs) from the small and large intestine ($n = 6-8$).

large intestinal IEC samples (Figure 2(a,c)). An examination at a finer taxonomic level showed that the proteobacterial species that increased most dramatically in *Ptpn2*-KO mice in these regional groups was an *Escherichia coli* phylotype (Figure 2(b,d)).

***PTPN2*-deficient mice harbor significant expansion of a novel *E. coli* phylotype with high sequence identity to AIECs**

To examine the relative abundance of this *E. coli* phylotype in these regional groups, edgeR analyses were performed. In the group comprised of the three regions of the large intestine lumen, the *E. coli* phylotype was more abundant in *Ptpn2*-KO mice compared with WT and Het mice (Figure 3(a)). The relative abundance of this *E. coli* phylotype was also significantly higher in *Ptpn2*-KO mice than in WT and Het mice in the group comprised of the IEC samples from the small and large intestine (Figure 3(b)).

Using NCBI BLAST, we determined that the rRNA ITS region (250 nucleotides) of the *E. coli* phylotype had 100% sequence identity with the first

described AIEC – the human clinical isolate, LF82, identified in Crohn’s disease patients.^{26,44} The key factor enabling us to identify this *E. coli* phylotype as a potential AIEC was our analysis of the bacterial rRNA ITS region.³⁶ When this sequence was first analyzed in 2015, there were only five exact matches in NCBI’s nucleotide (nt) database and one of them was LF82, suggesting that our *E. coli* phylotype could be an AIEC. Subsequent BLAST analyses of this *E. coli* rRNA ITS sequence in 2019 using NCBI’s nt database (updated on 2019/10/03 and excluding “Uncultured/environmental sample sequences”) identified 91 exact matches. Conversely, when we performed a similar analysis using a portion of the 16S rRNA gene (primers 515 F and 806 R, 253 nucleotides) of our isolated mouse *E. coli*, we obtained 12,352 identical matches. These data demonstrated the value of examining the rRNA ITS region of bacteria to identify our bacterium as a putative *E. coli*, and further provided the impetus for isolating this bacterium.³⁶ Since there is no genetic marker to conclusively distinguish AIEC from other *E. coli*, we next proceeded to confirm the phenotypic properties of our novel mouse *E. coli*.^{67,68}

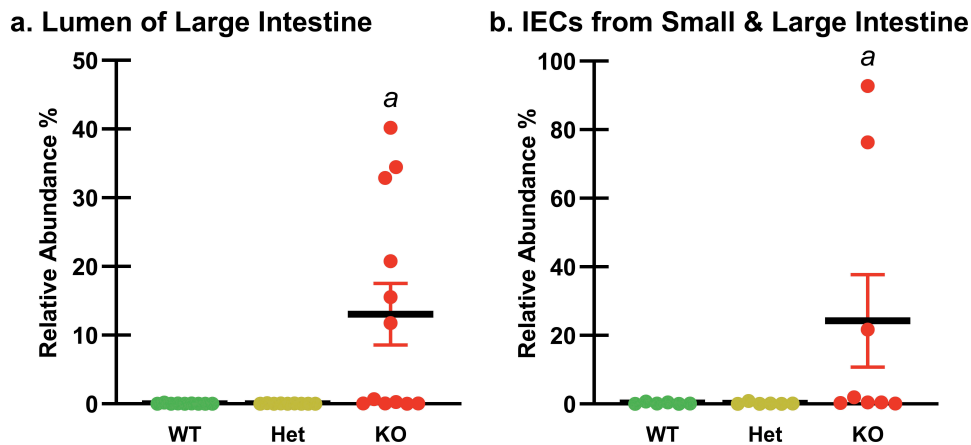


Figure 3. Relative Abundances of the *E. coli* Phylotype by Intestinal Region and *Ptpn2* Genotype. The relative abundances of the *E. coli* phylotype were examined in the regions identified by the beta diversity analysis (Figure 1(a)); (a) the lumen of the large intestine (cecum, proximal and distal colon) ($n = 9-12$), and (b) intestinal epithelial cells (IECs) from the small and large intestine ($n = 6-8$). Differences were determined using edgeR analyses at the species level. Data are shown as mean relative abundances (thick horizontal lines) \pm standard error. *Ptpn2*-KO mice showed higher relative abundance of *mAIEC* in the lumen of the large intestine ($^aP \leq 0.003$) and in IECs from the small and large intestine ($^aP < 0.001$) compared with WT and Het mice.

Confirmation of phenotypic properties of a novel mouse AIEC

Since AIEC have defined criteria to establish their adherent and invasive properties, we next determined if our *E. coli* isolate met these criteria in comparison to the human AIEC LF82 and the noninvasive *E. coli* K12.²³ Since, we did not observe any difference in bacterial adherence between human Caco-2BBE IECs and young-adult mouse colonic (YAMC) IECs (data not shown), we continued our studies using the better characterized Caco-2 cell line. Our *E. coli* isolate (*mAIEC*) showed greater adherence to and invasion of IECs than the control *E. coli* K12 (Figure 4(a-c)). Of note, the human LF82 AIEC adhered to and invaded human IECs at a much greater level than *mAIEC*. However, *mAIEC* showed greater infection of murine M ϕ (J774A.1) than the human LF82 AIEC and K12 (Figure 4(d-f)). These data confirm that our novel mouse *E. coli* is phenotypically an AIEC.

mAIEC colonizes and causes mild disease in SFB-free mice

We next tested whether our novel *mAIEC* colonizes mouse intestine and causes disease *in vivo* in the absence of SFB, since SFB is known to elicit a Th17 response which prevents AIEC colonization.⁶⁹ Whereas H₂O-PBS and H₂O-K12 mice showed

stable body weights, H₂O-*mAIEC* mice showed significant body weight loss at 4 and 7 days post infection compared with H₂O-PBS mice (Figure 5(a)). Interestingly, the drop in body weight coincided with a mild increase in disease activity index (DAI) with significantly higher DAI at day 4 and 5 post infection in H₂O-*mAIEC* mice compared with H₂O-PBS and H₂O-K12 mice (Figure 5(b)). H₂O-*mAIEC* mice showed no change in FD4 permeability (Figure 5(e)) or distal colon bacterial burden (see Figure 9(b)) on day 7 post-infection coinciding with normal DAI scores at day 7. However, H₂O-*mAIEC* mice showed increased spleen weight (Figure 5(c)), and colon shortening (Figure 5(d)) 7 d post infection compared with H₂O-PBS and H₂O-K12 mice. This observation could potentially be explained by the sustained fecal bacterial burden of *mAIEC* up to at least 15 d post infection (Suppl. Figure 2(a)). These data demonstrate that *mAIEC* caused mild and transient disease activity.

mAIEC requires a microbiome to invade germ-free mice

Having shown that *mAIEC* only caused transient disease in the presence of other gut bacteria, we next tested whether *mAIEC* alone caused disease by colonizing germ-free (GF) male and female mice with *mAIEC* or K12. Although *mAIEC*-infected

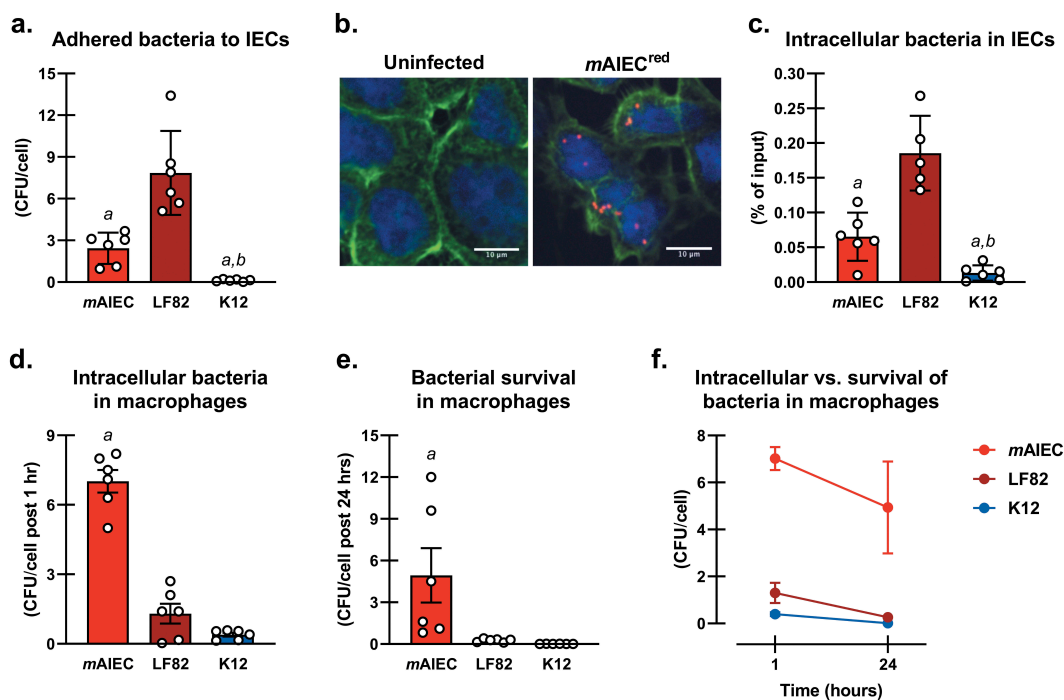


Figure 4. Confirmation of Phenotypic Properties of a Novel Mouse AIEC. Phenotypic characterization of a novel putative *mAIEC* compared with the human AIEC LF82 and the noninvasive *E. coli* K12. Caco-2BBE IECs (a,b,c) and J774A.1 murine macrophages (d,e,f) were seeded at 2×10^5 cells/well in a 24-well plate until confluent, or 5×10^5 cells/well on round coverslips until 70% confluent for (b), and then exposed for 3 h to individual bacteria (MOI of 10 bacteria/cell). 1-way ANOVA revealed interactions for all variables ($P \leq 0.004$; $n = 6$ from three independent experiments). (a) Bacteria adhered to Caco-2BBE cells as colony forming units (CFU)/cell ($^aP < 0.001$ cf. LF82, $^bP \leq 0.049$ cf. *mAIEC*); (b) Immunofluorescence of uninfected and *mAIEC^{red}* invaded Caco-2BBE cells ($n = 2-5$); (c) Intracellular bacteria as % of input in Caco-2BBE cells ($^aP < 0.001$ cf. LF82, $^bP \leq 0.03$ cf. *mAIEC*); (d) Intracellular bacteria as CFU/cell post 1 h in murine macrophages ($^aP < 0.001$ cf. all groups); (e) Survival of bacteria in murine macrophages as CFU/cell post 24 h ($^aP < 0.001$ cf. all groups); and (f) Relationship of intracellular bacteria and survival of bacteria in murine macrophages (no difference between *mAIEC* levels at 1 h vs. 24 h, $P = 0.49$). These data show that *mAIEC* attach to IECs, and can survive within macrophages, thus confirming AIEC properties.

mice showed fluctuations in body weight as early as 5 d post-infection compared with K12-colonized mice, this did not reach significance despite sustained *mAIEC* fecal bacterial burden (Figure 6, Suppl. Figure 2(b)). Interestingly, fecal microbiota transplant (FMT) of cecal content from a *Ptpn2*-KO mouse caused sustained, statistically significant, weight loss in mice compared with GF mice colonized with K12, and intriguingly, *mAIEC*-dependent weight loss was restricted to male GF mice (Figure 6). These data demonstrate that *mAIEC* is capable of causing disease only in the presence of other gastrointestinal microbes.

mAIEC worsens DSS colitis

We next wanted to determine if *mAIEC* modifies inflammation by worsening the response to an acute inflammatory episode. Whereas DSS control

mice (DSS-PBS or DSS-K12) did not show a significant loss in body weight, mice treated with DSS and infected with *mAIEC* (DSS-*mAIEC*) showed a significant and sustained drop in body weight beginning at 4 d compared with H₂O control mice (H₂O-PBS & H₂O-K12) and DSS-PBS mice, and 5–7 d compared with H₂O control mice and DSS treated (DSS-PBS, DSS-K12, DSS-*mAIEC*) mice (Figure 7(a)). Consequently, DSS-*mAIEC* mice showed severe disease indicated by a significant increase in DAI at 7 d, induction of splenomegaly, and a further shortening in colon length compared with H₂O control and DSS-treated mice (Figure 7(b–d)). Additionally, DSS-*mAIEC* mice showed a higher DAI, increased histological score, and MPO activity compared with DSS-PBS and DSS-K12 mice (Figures 7(e–f), 8).

As an additional determination of intestinal epithelial integrity and function, we assessed

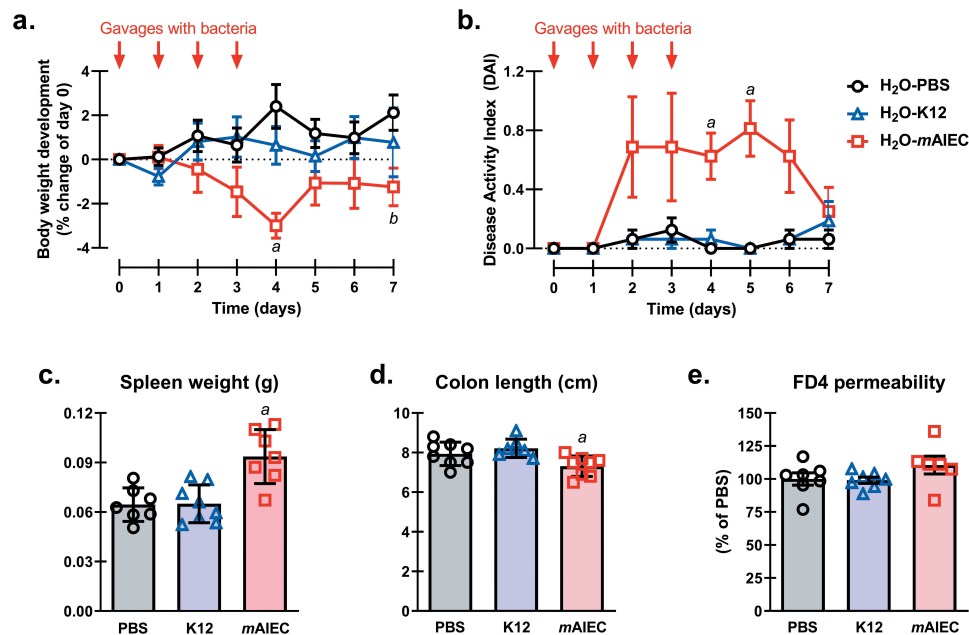


Figure 5. *mAIEC* Colonizes and Causes Mild Disease in SFB-free Mice. Oral gavage of *mAIEC* (10^9 bacteria/mouse in 100 μ L PBS; day 0–3) caused (a) weight loss ($n = 8$; also see Figure 7(a)); (b) mild disease ($n = 8$; also see Figure 8(b)); (c) splenomegaly ($n = 7$ –8; also see Figure 7(c)); (d) colon shortening ($n = 7$ –8; also see Figure 7(d)); and (e) intestinal FD4 permeability ($n = 6$ –7; also see Figure 8(a)) in confirmed SFB-free C57Bl/6 mice (10 weeks old; 20–22 g; JAX labs) compared with control *E. coli* (K12) or PBS after 7 d. 2-way repeated measures (RM) ANOVA of body weight and DAI revealed an interaction (mean \pm SEM from two independent experiments; $P \leq 0.002$). *mAIEC* reduced body weight at day 4 compared with all groups ($^aP \leq 0.01$) and day 7 compared with PBS ($^aP = 0.03$), and DAI at days 4 and 5 compared with all groups ($^aP \leq 0.02$). 1-way ANOVA of spleen weight and colon length, but not FD4 permeability revealed an interaction (mean \pm SD from two independent experiments; $P \leq 0.01$). *mAIEC* increased spleen weight compared with all groups ($^aP \leq 0.001$) and reduced colon length compared with K12 ($^aP \leq 0.01$).

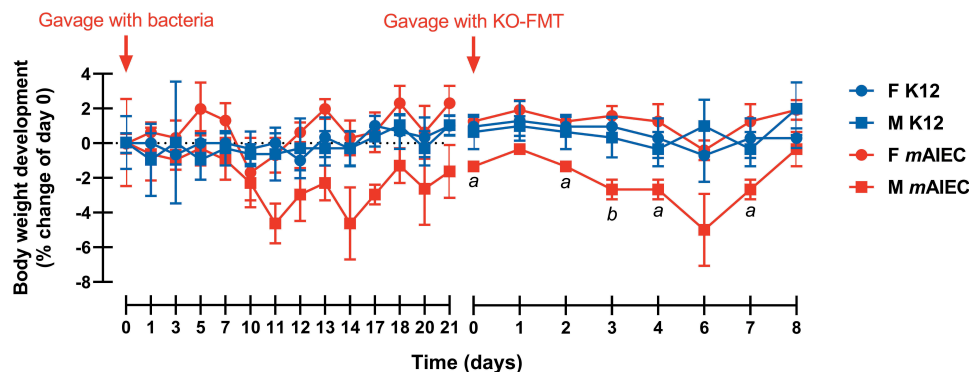


Figure 6. *mAIEC* Does Not Cause Disease in Germ-free Mice Without a Microbiome. Oral gavage of *mAIEC* (10^9 bacteria/mouse in 100 μ L PBS) to germ-free mice (C57Bl/6; 12–13 weeks old; $n = 3$, two experiments). Whereas *mAIEC* infection had no significant effect on body weight, fecal microbiota transplant (FMT) of cecal content from a *Ptpn2*-KO mouse (KO-FMT) by oral gavage after 21 d of *mAIEC* colonization caused a selective decrease in body weight in male vs. female *mAIEC*-infected mice while KO-FMT into control K12 *E. coli* infected mice was without effect ($n = 3$). 2-way RM ANOVA revealed an interaction (mean \pm SD; $P \leq 0.02$). Body weight of male *mAIEC* infected mice was significantly lower at days 0, 2, 4, and 7 post-KO-FMT compared with female *mAIEC* infected mice ($^aP \leq 0.02$) and at day 3 compared with female mice ($^bP \leq 0.005$).

in vivo permeability in the same mice used in Figures 7 and 8 and found that DSS-PBS, DSS-K12 and DSS-*mAIEC* mice showed increased permeability to FD4 compared with H₂O-PBS, H₂O-K12 or H₂O-*mAIEC* mice, and there was no

difference in FD4 permeability between DSS-*mAIEC* mice and DSS-PBS or DSS-K12 mice (Figure 9(a)). However, only DSS-*mAIEC* mice showed higher levels of bacterial burden in distal colon, spleen and liver compared with H₂O-PBS,

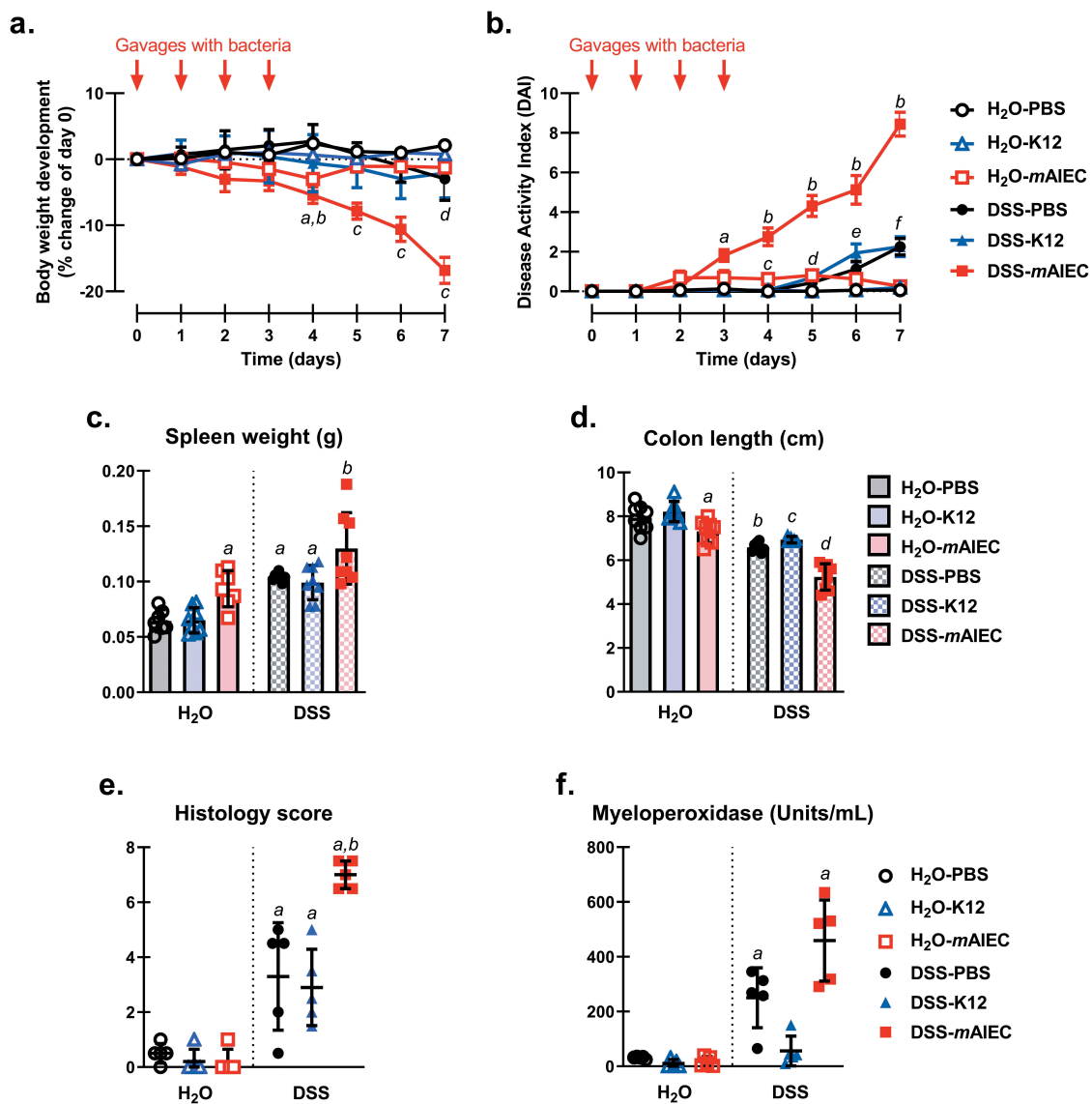


Figure 7. *mAIEC* Worsens Disease During Acute DSS Colitis. Co-administration of *mAIEC* and DSS (3%; 7 d) in drinking water exacerbated (a) weight loss ($n = 8$); (b) disease activity ($n = 8$); (c) splenomegaly ($n = 7-8$); (d) colon shortening ($n = 7-8$); (e) mean histology score ($n = 5$); and (f) MPO activity ($n = 5$) in confirmed SFB-free C57Bl/6 mice (10 weeks old; 20–22 g; JAX labs) compared with control *E. coli* (K12) or PBS. 2-way RM ANOVA of body weight and 1-way RM ANOVA of DAI revealed an interaction (mean \pm SEM from two independent experiments, $P < 0.001$). *mAIEC* alone in the absence of DSS caused a mild decrease in body weight (4 d, $^aP \leq 0.04$ cf. H₂O groups) and increase in DAI (4 d, $^cP \leq 0.04$ cf. H₂O-PBS and DSS-PBS; 5 d, $^dP \leq 0.04$ cf. H₂O groups). Although DSS-PBS mice showed a very mild decrease in body weight (7 d, $^dP \leq 0.03$ cf. H₂O-PBS) and increase in DAI (7 d, $^fP \leq 0.02$ cf. H₂O groups), and DSS-K12 mice showed an increase in DAI (6 d, $^eP \leq 0.03$ cf. H₂O-PBS and H₂O-K12; 7 d, $^fP \leq 0.04$ cf. H₂O groups), *mAIEC* potentiated the loss in body weight (4 d, $^bP = 0.02$ cf. H₂O-PBS and K12 and DSS-PBS; 5–7 d, $^aP \leq 0.04$ cf. all groups), and increased DAI (3 d, $^aP \leq 0.005$ cf. H₂O-PBS and K12 and DSS groups; 4–7 d, $^bP \leq 0.04$ cf. all groups). 1-way ANOVA of all other parameters revealed an interaction (mean \pm SD from two independent experiments except for mean histology score and MPO activity; $P \leq 0.001$). *mAIEC* alone in the absence of DSS and DSS-PBS and K12 equally caused splenomegaly ($^aP \leq 0.02$ cf. H₂O-PBS and K12). Additionally, *mAIEC* alone in the absence of DSS caused colon shortening ($^dP = 0.006$ cf. H₂O-K12). However, DSS-PBS and K12 showed more pronounced shortening of the colon ($^bP \leq 0.03$ cf. H₂O groups and $^cP \leq 0.005$ cf. H₂O-PBS and K12, respectively). *mAIEC* further potentiated the increase in spleen weight ($^bP \leq 0.04$ cf. all groups) and colon shortening ($^dP \leq 0.001$ cf. all groups). All DSS-treated mice showed an increase in mean histology score ($^aP \leq 0.02$ cf. H₂O groups) and this effect was worsened when DSS mice were infected with *mAIEC* ($^bP \leq 0.001$ cf. DSS groups). MPO activity was increased in DSS-PBS but not DSS-K12 mice, and this effect was not worsened when DSS mice were infected with *mAIEC* ($^aP \leq 0.008$ cf. all groups).

H₂O-K12 and H₂O-*mAIEC* mice and DSS-PBS and DSS-K12 mice (Figure 9(b–d)). Interestingly, there

was no significant bacterial burden found in mesenteric lymph nodes (mLN) (data not shown).

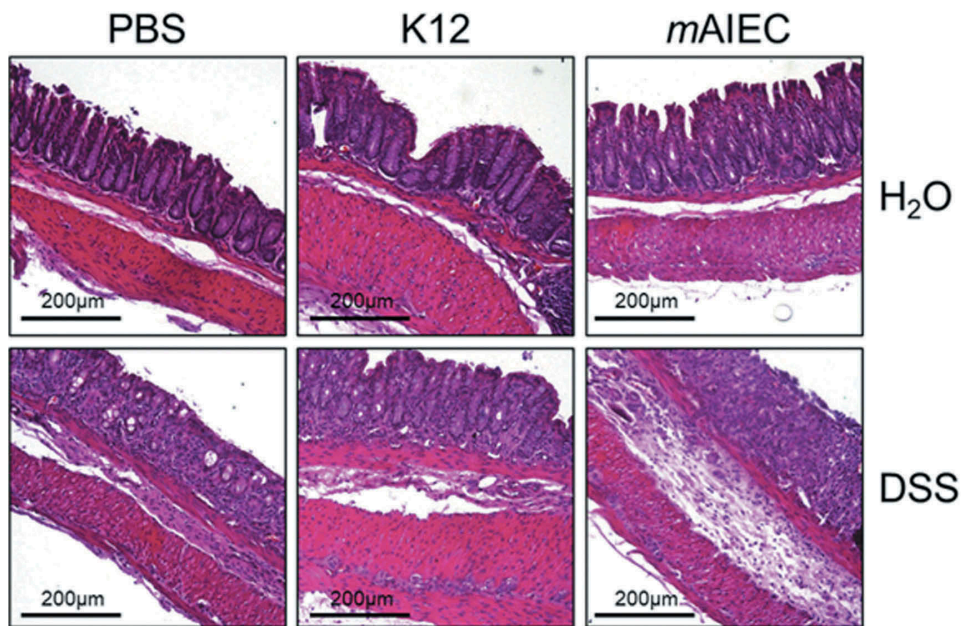


Figure 8. Histology of Distal Colons from Colitis Mice Infected with *E. coli*. Hematoxylin and Eosin stained sections ($5\ \mu\text{M}$) of the most distal 1 cm of the mouse colon from water treated or DSS-colitis mice gavaged with PBS, control *E. coli* K12, or *mAIEC*.

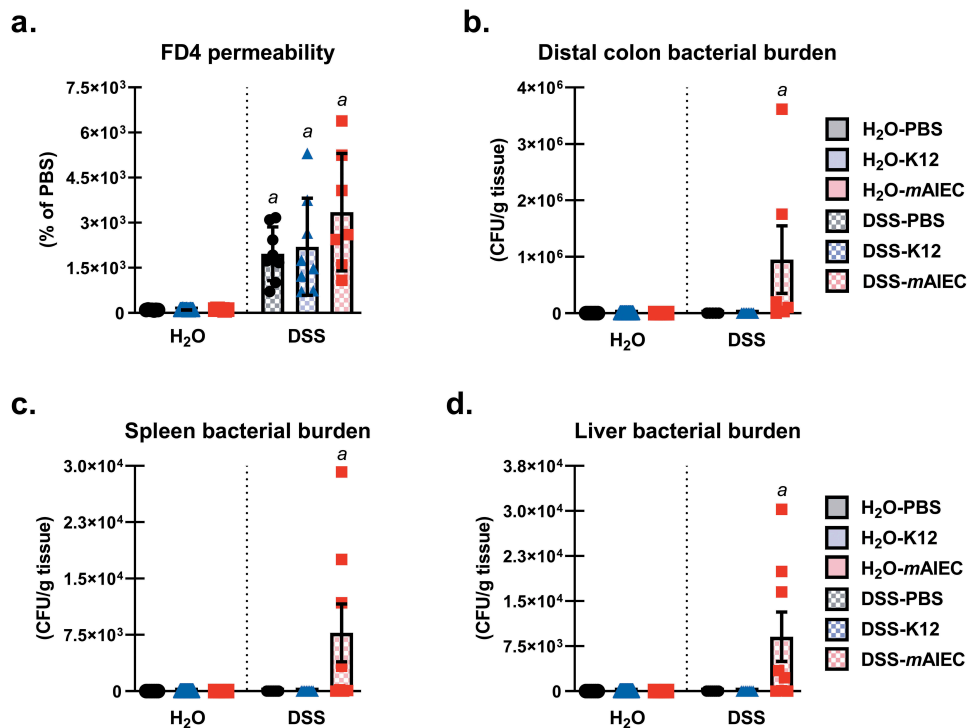


Figure 9. *mAIEC* Infection During DSS Worsens Barrier Permeability and Increases Bacterial Burden. Co-administration of *mAIEC* and DSS (3%; 7 d) in drinking water exacerbated (a) FD4 permeability (as % of H_2O -PBS; $n = 6-8$); and bacterial burden of *mAIEC* in the (b) distal colon ($n = 5-8$); (c) spleen ($n = 6-8$); and (d) liver ($n = 6-8$) in confirmed SFB-free C57Bl/6 mice (10 weeks old; 20–22 g) compared with control *E. coli* (K12) or PBS. 2-way ANOVA revealed an interaction (mean \pm SD from two independent experiments; $P \leq 0.03$). DSS induced an increase in permeability independent of infection ($^aP = 0.01$ cf. H_2O mice) and there was no difference between the DSS mice ($P \geq 0.13$). DSS-*mAIEC* mice had greater bacterial burden in their distal colon ($^aP \leq 0.04$ cf. DSS-K12 mice), spleen ($^aP \leq 0.03$ cf. all mice), and liver ($^aP \leq 0.02$ cf. all mice).

Overall, these data confirm that *mAIEC*: (i) invades SFB-free mouse intestine, (ii) causes disease and weight loss; (iii) increases intestinal permeability; and (iv) exacerbates disease in the setting of inflammation.

mAIEC prevents recovery from DSS colitis

Since *mAIEC* worsened acute colitis, we wanted to determine if it also impaired recovery from colitis.

DSS-induced colitis in all of the mice in the recovery group, regardless of bacterial infection, as evidenced by reduced body weight; however, mice infected with *mAIEC* during the recovery phase (*rec-mAIEC*) showed a more severe body weight loss and slower recovery at 13 and 14 d compared with mice treated with PBS (*rec-PBS*) and mice infected with K12 (*rec-K12*) during the recovery phase (Figure 10(a)). Consequently, *rec-mAIEC* mice showed a higher and more sustained DAI

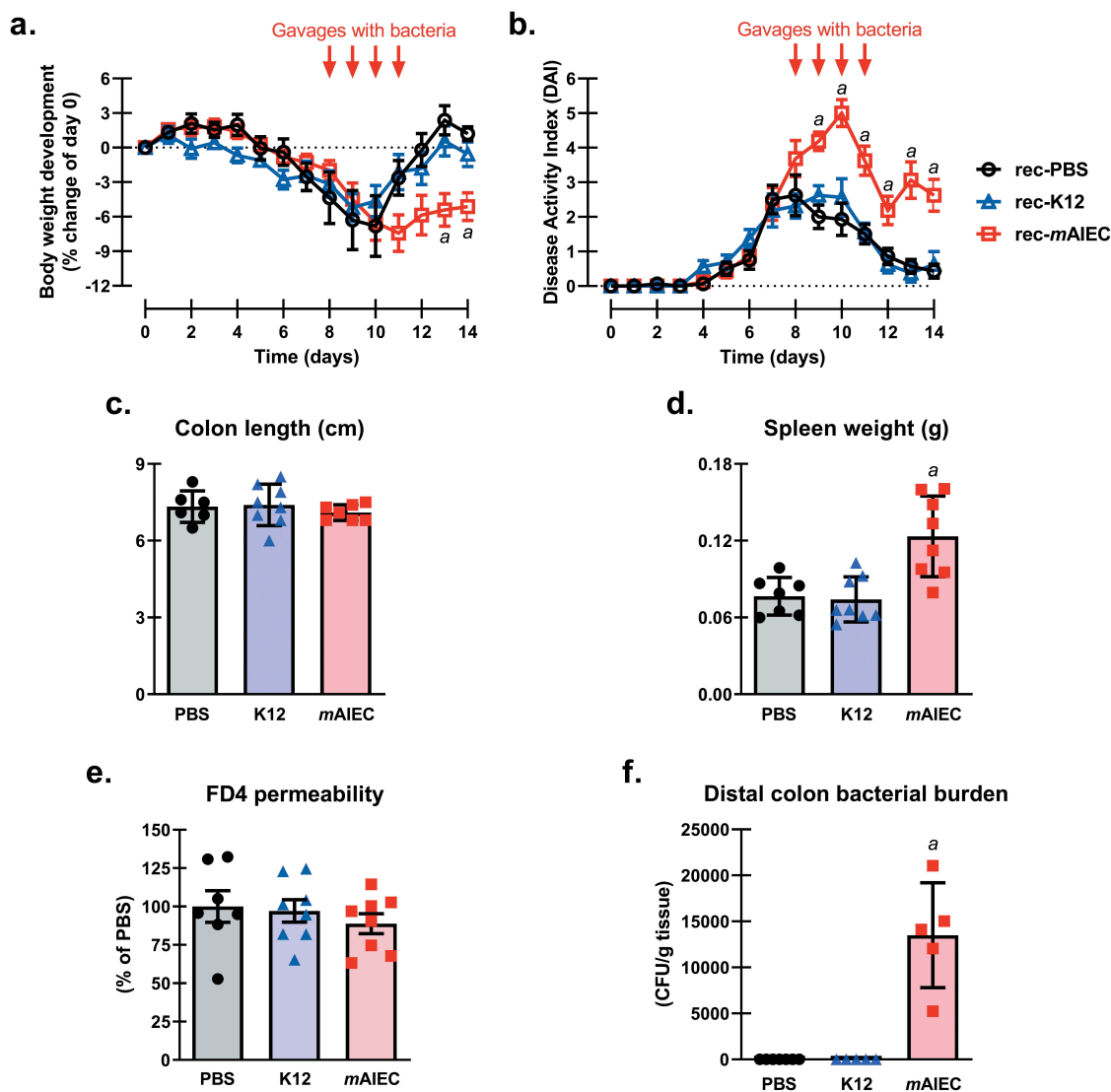


Figure 10. *mAIEC* Impairs Recovery from Colitis. Administration of *mAIEC* post DSS (3%; 7 d) in drinking water impaired recovery of (a) body weight ($n = 7-8$); (b) disease ($n = 7-8$); and (d) splenomegaly ($n = 7-8$); with no effect on (c) colon length ($n = 6-8$); (e) FD4 permeability (as % of *rec-PBS*; $n = 7-8$); or (f) bacterial burden ($n = 5-8$) of *mAIEC* to the distal colon in confirmed SFB-free C57Bl/6 mice (10 weeks old; 20–22 g; JAX labs) compared with control *E. coli* (K12) or PBS. 2-way RM ANOVA of body weight and DAI revealed an interaction (mean \pm SEM from two independent experiments; $P < 0.001$). *mAIEC* prevented recovery of body weight loss (13–14 d, $^aP \leq 0.03$ cf. *rec-PBS* and K12), and decrease in DAI (9–14 d, $^aP \leq 0.03$ cf. *rec-PBS* and K12). One-way ANOVA of spleen weight and distal colon bacterial burden revealed an interaction (mean \pm SEM from two independent experiments; $P < 0.001$) with no effect on colon length or FD4 permeability ($^aP \geq 0.59$). *mAIEC* increased spleen weight during the recovery phase ($^aP \leq 0.002$ cf. *rec-PBS* and K12) and was detected in distal colon tissue ($^aP \leq 0.001$ cf. *rec-PBS* and K12).

from day 9 through 14 compared with rec-PBS and rec-K12 mice (Figure 10(b)). This coincided with splenomegaly and bacterial burden in distal colon but no change in colon length or FD4 permeability in rec-*mAIEC* mice compared with rec-PBS and rec-K12 mice (Figure 10(c–f)). Overall, these data show that *mAIEC* prevents recovery of acute colitis.

Genome sequence analysis of *mAIEC*

Since the rRNA ITS region of *mAIEC* and the human AIEC LF82 had 100% sequence identity, we next wanted to identify how similar these bacteria are across their genomes. We sequenced the genome of our novel mouse AIEC and compared it with the published genome sequence of LF82 (GenBank CU651637.1). *mAIEC* showed approximately 90.3% sequence identity to the genome of the human AIEC LF82. We further probed for the presence in our *mAIEC* of putative virulence genes found in *E. coli*'s and other AIECs including LF82. Putative virulence gene sequences and their predicted protein products were compared using EMBOSS Water (Table 1).^{63,64} There were 14 total

putative virulence genes that were used in this analysis. In particular, *mAIEC* showed two distinct differences: *mAIEC yfcU* and *tnpB* had very low % gene and protein identities when compared to the same gene and protein sequences from LF82 and NC101 (Table 1). Since analyses using BLAST determined that the closest matches to these genes and proteins were *yfcU* or *tnpB* for all three bacteria, this suggests that these proteins all have similar functions but that the sequences from our *mAIEC* are very different from those from LF82 and NC101.

Discussion

One of the contributing factors to IBD development and progression is alteration of intestinal microbiome composition that favors expansion of commensal bacteria with potential to cause disease. In mice with loss of expression of the IBD risk gene, *Ptpn2*, we found significant alterations in intestinal bacteria compared with wild-type littermates. Moreover, *Ptpn2*-deficient mice showed a selective increase in abundance of *Proteobacteria*, specifically

Table 1. Summary of Putative Virulence Genes Between the Novel *mAIEC*, LF82 AIEC and NC101 *E. coli*.

Gene	Reference	Function	% gene identity with NC101	% query covered	% putative protein identity with NC101	% query covered	% gene identity with LF82 (Accession CU651637.1)	% query covered	% putative protein identity with LF82	% query covered
<i>fimH</i>	⁷⁰	Terminal subunit of Type 1 pilus	*99.1	100	99	100	99.4	100	99.5	100
<i>yfcU</i>	⁷¹	Outer membrane usher protein	55.5	98	44.6	97	54.7	87	44.7	97
<i>yadC</i>	⁷²	Fimbrial-like protein	*92.8	100	91.2	100	*93.2	100	91.2	100
<i>csgE</i>	⁷³	Curli production assembly/transport component	99.7	100	100	100	99.7	100	100	100
<i>yehA</i>	⁷⁴	Putative fimbrial-like protein	99.3	100	99.4	100	99.4	100	99.4	100
<i>hcpA</i>	⁷³	Major exported protein	98.6	100	100	100	100	100	100	100
<i>fimA</i>	⁷³	Type-1 fimbrial protein A chain	90.2	100	90.7	100	*91.4	100	91.3	100
<i>ygiL</i>	⁷⁵	Fimbrial family protein	100	100	100	100	100	100	100	100
<i>ftsh</i>	⁷⁶	ATP-dependent zinc metalloprotease	99.3	100	100	100	99.3	100	100	100
<i>vat</i>	⁷⁷	Vacuolating autotransporter toxin	100	100	100	100	100	100	100	100
<i>malX</i>	⁷³	PTS system maltose- and glucose- specific EIICB component	99.7	99	100	100	99.7	100	100	100
<i>tnpB</i>	⁷⁸	IS200/IS605 family element transposase accessory protein	43.5	99	34.1	93	47.6	99	34.1	94
<i>dsbA</i>	⁷³	Thiol:disulfide interchange protein	99.4	100	100	100	99.7	100	100	100
<i>fliA</i>	⁷⁹	RNA polymerase sigma factor	98.9	100	100	100	99.8	100	100	100

*For the indicated gene comparisons, when the % gene identity was greater than % protein identity, there was a higher percentage of nucleotide differences in codon positions 1 + 2 (32%) than when % gene identity was less than % protein identity (9%). Similar comparisons of the genes with equal % identities and the two genes with much greater dissimilarities (*yfcU* and *tnpB*) were not included in this analysis.

E. coli. Intriguingly, the highest increase in abundance of luminal and mucosal-associated bacteria in *Ptpn2*-KO mice was of an *E. coli* that shared >90% genome sequence similarity to the human IBD-associated AIEC LF82. Furthermore, IBD patients that have been genotyped for the *PTPN2* IBD risk allele rs1893217 show altered microbiomes and increased presence of *Proteobacteria*, thus further validating our *in vivo* system as a model of IBD.^{23,33,34} Although LF82 was originally isolated from the ileum of a Crohn's disease patient, additional AIEC have since been identified in ulcerative colitis patients and isolated from other intestinal regions.^{37,80-82} Whereas *m*AIEC was detected albeit at low levels in luminal and mucosal-associated samples from wild-type mice indicating that this bacterium is part of the resident microbiota, *Ptpn2*-KO mice showed higher abundance of *m*AIEC in both the lumen of the gut and the epithelium of the small and large intestine. This was a notable finding because IBD-associated AIEC are able to adhere to and invade IECs. Moreover, the finding that our novel *m*AIEC was present in IECs *in vivo* further supports its identity as an AIEC. Overall, reduced expression of the IBD candidate gene, *Ptpn2*, alters intestinal microbial communities in mice to favor expansion of this novel mouse AIEC.

We confirmed the adherent, invasive and survival properties of *m*AIEC relative to the well-studied human AIEC LF82.²³ We found that *m*AIEC adhere to and invade intestinal epithelial cells, although to a lesser extent than LF82. This was expected as we used human IECs with a mouse bacterium to comply with the criteria for identification as AIEC that were established for LF82.²³ However, the absolute values of *m*AIEC adherence and invasion are not significantly different from the published adherence and invasive properties for an AIEC, and there was no difference in adherence of *m*AIEC to young adult mouse colonic (YAMC) IEC lines compared with human IECs.^{23,26} Intriguingly, survival of *m*AIEC in J774A.1 mouse macrophages was significantly higher than LF82 and K12, and this was not solely a host-specific effect since *m*AIEC invaded human THP-1 macrophages similar to LF82 (Spalinger et al., unpublished manuscript; under review). Given that our current studies were performed with mouse macrophages, this may suggest that our novel *m*AIEC

represents a better tool to study AIEC-induced disease in a mouse host than the human LF82 isolate. Overall, these data confirm the epithelial adherent and invasive properties and survival in macrophages of our novel *m*AIEC.

We also validated that our novel mouse AIEC can cause disease in SFB-free mice. These mice were housed under SPF conditions reflecting the housing conditions of the *Ptpn2*-KO mice in which we found a high abundance of *m*AIEC (SPF mice with low abundance of SFB, data not shown). We confirmed that infection of *m*AIEC, but not K12, results in mild disease evident by reduced body weight and slightly increased disease activity. The lack of an overt response to infection, and that these mice appear to recover by day 7 despite delayed recovery of spleen weight and colon length due to pathologic changes to the tissue, may be explained by the fact that these mice already have a microbiome that could partially outcompete or restrict *m*AIEC pathogenicity.⁸³ Therefore, we infected germ-free mice and found that mono-colonization with *m*AIEC had no significant effect on body weight despite sustained levels of bacterial burden. Interestingly, introduction of a microbiome by FMT in *m*AIEC-infected germ-free mice caused a significant and sustained reduction in body weight, and intriguingly, this effect seemed to be specific to male mice despite similar *m*AIEC and K12 bacterial burden levels in male and female germ-free mice pre-FMT. However, female mice also showed large fluctuations in body weight indicating that *m*AIEC resulted in a response in both male and female germ-free mice albeit with qualitative differences in the magnitude of the effect that appears to be sex-dependent. We showed for the first time that our *m*AIEC (a pathobiont) can cause transient disease in mice with no known genetic alterations or additional stressors such as DSS-induced colitis.

Since we isolated *m*AIEC from *Ptpn2*-KO mice that develop systemic inflammation, and since AIEC have been shown to be increased in CD and UC patients, we investigated the effects of *m*AIEC in an inflammatory setting. Mice exposed to DSS to induce mild colitis and simultaneously infected with *m*AIEC displayed more severe disease (greater body weight loss, increased disease scores, bacterial burden) compared with control mice treated with

DSS and water treated mice; and increased macromolecular intestinal permeability compared with water-treated mice. We speculate that inflammation is required in the host to create an ideal environment for AIEC to expand and cause a more severe and sustained disease, consistent with it being a pathobiont (such as the human LF82 AIEC) rather than a strict pathogen.⁸⁴ In fact, AIEC have been shown to worsen the response to an inflammatory flare, and impede a susceptible host from recovery against acute colitis in IBD patients, thus potentiating IBD progression.^{84,85} Of note, mice infected with *mAIEC* fail to recover (body weight loss and increased disease activity) from DSS-induced colitis.

To identify possible factors that contribute to *mAIEC* colonization in mice, we compared the genome sequence of the novel mouse AIEC to the human LF82 AIEC and another opportunistic mouse *E. coli* with some AIEC features, NC101. The genome of *mAIEC* showed >90% sequence identity to LF82. Intriguingly, two putative virulence genes, *yfcU* and *tnpB*, from our *mAIEC* were compared to those from LF82 and NC101. The *mAIEC* gene and putative protein sequences had very low percent identities when compared to the other two bacteria providing further evidence for the novelty of our strain and indicating potentially different gene variants or protein isoforms that may give rise to differences in pathogenicity (e.g., adherence/invasion) between *mAIEC*, LF82 and NC101.

While a number of studies have investigated potential contributions of commensal bacteria that possess or acquire pathogenic potential, such as the LF82 AIEC in the pathogenesis of IBD, it still remains elusive as to how IBD susceptibility genes modulate the intestinal microbiome to maintain intestinal homeostasis and how disruption of this interaction precipitates changes in the microbiome that promote disease. We show here for the first time how loss of an IBD-associated gene, *Ptpn2*, in mice (*Ptpn2*-deficient), independent of an external stressor, alters the intestinal microbiome and favors expansion of a novel mouse AIEC that is capable of both initiating and exacerbating disease. Thus, *PTPN2* plays a key role as a “microbial modulator” of the microbiome to protect against pathobiont expansion and colonization. We propose that

whole-body *Ptpn2*-deficiency in mice may serve as a useful model to investigate how host genetics modulate the balance of intestinal microbes, and that this novel mouse AIEC can be utilized to interrogate mechanisms of pathobiont-induced intestinal inflammation.

Acknowledgments

We are grateful to Dr. Jason Stajich (UCR) for valuable discussions. We are grateful to Dr. David Lo (UCR) for providing access to the CSU-X-1 spinning-disk confocal imager.

Disclosure of Potential Conflicts of Interest

The authors report no conflicts of interest.

Funding

This work was supported by a Crohn's and Colitis Foundation Research Fellowship Award (A.S.); Crohn's and Colitis Foundation Senior Research Award (D.F.M.); NIH-2R01-DK091281 (D.F.M.); American Gastroenterological Association IBD Research Award (D.F.M.); UCR Office of Research & Economic Development Pilot Award (D.F.M. & J.B.); National Institute of General Medical Sciences grant R35GM124724 (to A.H.).

ORCID

Ali Shawki  <http://orcid.org/0000-0002-6413-5313>

Alina N. Santos  <http://orcid.org/0000-0002-9041-7250>

Vinicius Canale  <http://orcid.org/0000-0002-2030-0268>

Michel L. Tremblay  <http://orcid.org/0000-0002-0281-541X>

Declan F. McCole  <http://orcid.org/0000-0002-6286-0802>

References

1. Jostins L, Ripke S, Weersma RK, Duerr RH, McGovern DP, Hui KY, Lee JC, Schumm LP, Sharma Y, Anderson CA, et al. Host-microbe interactions have shaped the genetic architecture of inflammatory bowel disease. *Nature*. 2012;491(7422):119–124.
2. Franke A, Balschun T, Karlsen TH, Hedderich J, May S, Lu T, Schuldt D, Nikolaus S, Rosenstiel P, Krawczak M, et al. Replication of signals from recent studies of Crohn's disease identifies previously unknown disease loci for ulcerative colitis. *Nat Genet*. 2008;40(6):713–715. doi:10.1038/ng.148.
3. Wellcome Trust Case Control Study C. Genome-wide association study of 14,000 cases of seven common

- diseases and 3,000 shared controls. *Nature*. 2007;447(7145):661–678. doi:10.1038/nature05911.
4. Spalinger MR, Voegelin M, Biedermann L, Zeitz J, Rossel JB, Sulz MC, Frei P, Scharl S, Vavricka SR, Fried M, et al. The clinical relevance of the IBD-associated variation within the risk gene locus encoding protein tyrosine phosphatase non-receptor type 2 in patients of the Swiss IBD Cohort. *Digestion*. 2016;93(3):182–192. doi:10.1159/000444479.
 5. Smyth DJ, Plagnol V, Walker NM, Cooper JD, Downes K, Yang JHM, Howson JMM, Stevens H, McManus R, Wijmenga C, et al. Shared and distinct genetic variants in type 1 diabetes and celiac disease. *N Engl J Med*. 2008;359(26):2767–2777. doi:10.1056/NEJMoa0807917.
 6. Khor B, Gardet A, Xavier RJ. Genetics and pathogenesis of inflammatory bowel disease. *Nature*. 2011;474(7351):307–317. doi:10.1038/nature10209.
 7. You-Ten KE, Muise ES, Itie A, Michaliszyn E, Wagner J, Jothy S, Lapp WS, Tremblay ML. Impaired bone marrow microenvironment and immune function in T cell protein tyrosine phosphatase-deficient mice. *J Exp Med*. 1997;186(5):683–693. doi:10.1084/jem.186.5.683.
 8. Heinonen KM, Nestel FP, Newell EW, Charette G, Seemayer TA, Tremblay ML, Lapp WS. T-cell protein tyrosine phosphatase deletion results in progressive systemic inflammatory disease. *Blood*. 2004;103(9):3457–3464. doi:10.1182/blood-2003-09-3153.
 9. Yamamoto T, Sekine Y, Kashima K, Kubota A, Sato N, Aoki N, Matsuda T. The nuclear isoform of protein-tyrosine phosphatase TC-PTP regulates interleukin-6-mediated signaling pathway through STAT3 dephosphorylation. *Biochem Biophys Res Commun*. 2002;297(4):811–817. doi:10.1016/S0006-291X(02)02291-X.
 10. Krishnan M, McCole DF. T cell protein tyrosine phosphatase prevents STAT1 induction of claudin-2 expression in intestinal epithelial cells. *Ann N Y Acad Sci*. 2017;1405(1):116–130. doi:10.1111/nyas.13439.
 11. Scharl M, Paul G, Weber A, Jung BC, Docherty MJ, Hausmann M, Rogler G, Barrett KE, McCole DF. Protection of epithelial barrier function by the Crohn's disease associated gene protein tyrosine phosphatase n2. *Gastroenterology*. 2009;137(6):2030–2040. doi:10.1053/j.gastro.2009.07.078.
 12. Matter K, Balda MS. Signalling to and from tight junctions. *Nat Rev Mol Cell Biol*. 2003;4(3):225–236. doi:10.1038/nrm1055.
 13. Shen L, Weber CR, Raleigh DR, Yu D, Turner JR. Tight junction pore and leak pathways: a dynamic duo. *Annu Rev Physiol*. 2011;73:283–309. doi:10.1146/annurev-physiol-012110-142150.
 14. Assimakopoulos SF, Triantos C, Thomopoulos K, Fligou F, Maroulis I, Marangos M, Gogos CA. Gut-origin sepsis in the critically ill patient: pathophysiology and treatment. *Infection*. 2018;46(6):751–760. doi:10.1007/s15010-018-1178-5.
 15. Guerville M, Boudry G. Gastrointestinal and hepatic mechanisms limiting entry and dissemination of lipopolysaccharide into the systemic circulation. *Am J Physiol Gastrointest Liver Physiol*. 2016;311(1):G1–G15. doi:10.1152/ajpgi.00098.2016.
 16. Bein A, Zilbershtein A, Golosovsky M, Davidov D, Schwartz B. LPS induces hyper-permeability of intestinal epithelial cells. *J Cell Physiol*. 2017;232(2):381–390. doi:10.1002/jcp.25435.
 17. Chowdhury SR, King DE, Willing BP, Band MR, Beever JE, Lane AB, Loor JJ, Marini JC, Rund LA, Schook LB, et al. Transcriptome profiling of the small intestinal epithelium in germfree versus conventional piglets. *BMC Genomics*. 2007;8:215. doi:10.1186/1471-2164-8-215.
 18. Ghoshal UC, Shukla R, Ghoshal U, Gwee KA, Ng SC, Quigley EMM. The gut microbiota and irritable bowel syndrome: friend or foe? *Int J Inflam*. 2012;2012:151085. doi:10.1155/2012/151085.
 19. Sender R, Fuchs S, Milo R. Revised estimates for the number of human and bacteria cells in the body. *PLoS Biol*. 2016;14(8):e1002533. doi:10.1371/journal.pbio.1002533.
 20. Stecher B. The roles of inflammation, nutrient availability and the commensal microbiota in enteric pathogen infection. In: Conway T, Cohen PS, editors. *Metabolism and bacterial pathogenesis*; Washington (DC): SM Press; 2015. p. 297–320. doi:10.1128/microbiolspec.MBP-0008-2014.
 21. Rogler G, Luc B, Scharl M. New insights into the pathophysiology of inflammatory bowel disease: microbiota, epigenetics and common signalling pathways. *Swiss Med Wkly*. 2018;148:w14599. doi:10.4414/sm.w.2018.14575.
 22. Craven M, Egan CE, Dowd SE, McDonough SP, Dogan B, Denkers EY, Bowman D, Scherl EJ, Simpson KW. Inflammation drives dysbiosis and bacterial invasion in murine models of ileal Crohn's disease. *PLoS One*. 2012;7(7):e41594. doi:10.1371/journal.pone.0041594.
 23. Martinez-Medina M, Garcia-Gil LJ. *Escherichia coli* in chronic inflammatory bowel diseases: an update on adherent invasive *Escherichia coli* pathogenicity. *World J Gastrointest Pathophysiol*. 2014;5(3):213–227. doi:10.4291/wjgp.v5.i3.213.
 24. Chassaing B, Koren O, Carvalho FA, Ley RE, Gewirtz AT. AIEC pathobiont instigates chronic colitis in susceptible hosts by altering microbiota composition. *Gut*. 2014;63(7):1069–1080. doi:10.1136/gutjnl-2013-304909.
 25. Carvalho FA, Koren O, Goodrich JK, Johansson MEV, Nalbantoglu I, Aitken JD, Su Y, Chassaing B, Walters WA, Gonzalez A, et al. Transient inability to manage proteobacteria promotes chronic gut inflammation in TLR5-deficient mice. *Cell Host Microbe*. 2012;12(2):139–152. doi:10.1016/j.chom.2012.07.004.
 26. Darfeuille-Michaud A, Boudeau J, Bulois P, Neut C, Glasser AL, Barnich N, Bringer MA, Swidsinski A,

- Beaugerie L, Colombel JF. High prevalence of adherent-invasive *Escherichia coli* associated with ileal mucosa in Crohn's disease. *Gastroenterology*. 2004;127(2):412–421. doi:10.1053/j.gastro.2004.04.061.
27. Eaves-Pyles T, Allen CA, Taormina J, Swidsinski A, Tutt CB, Jezek GE, Islas-Islas M, Torres AG. *Escherichia coli* isolated from a Crohn's disease patient adheres, invades, and induces inflammatory responses in polarized intestinal epithelial cells. *Int J Med Microbiol*. 2008;298(5–6):397–409. doi:10.1016/j.ijmm.2007.05.011.
28. Berkes J, Viswanathan VK, Savkovic SD, Hecht G. Intestinal epithelial responses to enteric pathogens: effects on the tight junction barrier, ion transport, and inflammation. *Gut*. 2003;52(3):439–451. doi:10.1136/gut.52.3.439.
29. Shawki A, McCole DF. Mechanisms of intestinal epithelial barrier dysfunction by adherent-invasive *Escherichia coli*. *Cell Mol Gastroenterol Hepatol*. 2017;3(1):41–50. doi:10.1016/j.jcmgh.2016.10.004.
30. Liao AP, Petrof EO, Kuppireddi S, Zhao Y, Xia Y, Claud EC, Sun J. Salmonella type III effector AvrA stabilizes cell tight junctions to inhibit inflammation in intestinal epithelial cells. *PLoS One*. 2008;3(6):e2369. doi:10.1371/journal.pone.0002369.
31. Ulluwishewa D, Anderson RC, McNabb WC, Moughan PJ, Wells JM, Roy NC. Regulation of tight junction permeability by intestinal bacteria and dietary components. *J Nutr*. 2011;141(5):769–776. doi:10.3945/jn.110.135657.
32. Molodecky NA, Kaplan GG. Environmental risk factors for inflammatory bowel disease. *Gastroenterol Hepatol (N Y)*. 2010;6:339–346.
33. Knights D, Silverberg MS, Weersma RK, Gevers D, Dijkstra G, Huang H, Tyler AD, van Sommeren S, Imhann F, Stempak JM, et al. Complex host genetics influence the microbiome in inflammatory bowel disease. *Genome Med*. 2014;6(12):107. doi:10.1186/s13073-014-0107-1.
34. Yilmaz B, Spalinger MR, Biedermann L, Franc Y, Fournier N, Rossel JB, Juillerat P, Rogler G, Macpherson AJ, Scharl M. The presence of genetic risk variants within PTPN2 and PTPN22 is associated with intestinal microbiota alterations in Swiss IBD cohort patients. *PLoS One*. 2018;13(7):e0199664. doi:10.1371/journal.pone.0199664.
35. Spalinger MR, Kasper S, Chassard C, Raselli T, Frey-Wagner I, Gottier C, Lang S, Atrott K, Vavricka SR, Mair F, et al. PTPN22 controls differentiation of CD4(+) T cells and limits intestinal inflammation and intestinal dysbiosis. *Mucosal Immunol*. 2015;8(4):918–929. doi:10.1038/mi.2014.122.
36. Ruegger PM, Clark RT, Weger JR, Braun J, Borneman J. Improved resolution of bacteria by high throughput sequence analysis of the rRNA internal transcribed spacer. *J Microbiol Methods*. 2014;105:82–87. doi:10.1016/j.mimet.2014.07.001.
37. Darfeuille-Michaud A, Neut C, Barnich N, Lederman E, Di Martino P, Desreumaux P, Gambiez L, Joly B, Cortot A, Colombel JF. Presence of adherent *Escherichia coli* strains in ileal mucosa of patients with Crohn's disease. *Gastroenterology*. 1998;115(6):1405–1413. doi:10.1016/S0016-5085(98)70019-8.
38. Presley LL, Wei B, Braun J, Borneman J. Bacteria associated with immunoregulatory cells in mice. *Appl Environ Microbiol*. 2010;76(3):936–941. doi:10.1128/AEM.01561-09.
39. Fujiwara D, Chen L, Wei B, Braun J. Small intestine CD11c+ CD8+ T cells suppress CD4+ T cell-induced immune colitis. *Am J Physiol Gastrointest Liver Physiol*. 2011;300(6):G939–G947. doi:10.1152/ajpgi.00032.2010.
40. Tannock GW, Crichton CM, Savage DC. A method for harvesting non-cultivable filamentous segmented microbes inhabiting the ileum of mice. *FEMS Microbiol Lett*. 1987;45(6):329–332. doi:10.1111/j.1574-6968.1987.tb02409.x.
41. Ginnan NA, Dang T, Bodaghi S, Ruegger PM, Peacock BB, McCollum G, England G, Vidalakis G, Roper C, Rolshausen P, et al. Bacterial and fungal next generation sequencing datasets and metadata from citrus infected with 'candidatus liberibacter asiaticus'. *Phytobiomes*. 2018;2:64–70. doi:10.1094/PBIOMES-08-17-0032-A.
42. Edgar RC. UPARSE: highly accurate OTU sequences from microbial amplicon reads. *Nat Methods*. 2013;10(10):996–998. doi:10.1038/nmeth.2604.
43. Edgar RC. UNOISE2: improved error-correction for Illumina 16S and ITS amplicon sequencing. *bioRxiv*. 2016;081257.
44. Altschul SF, Gish W, Miller W, Myers EW, Lipman DJ. Basic local alignment search tool. *J Mol Biol*. 1990;215(3):403–410. doi:10.1016/S0022-2836(05)80360-2.
45. Lozupone CA, Hamady M, Kelley ST, Knight R. Quantitative and qualitative beta diversity measures lead to different insights into factors that structure microbial communities. *Appl Environ Microbiol*. 2007;73(5):1576–1585. doi:10.1128/AEM.01996-06.
46. Caporaso JG, Kuczynski J, Stombaugh J, Bittinger K, Bushman FD, Costello EK, Fierer N, Pena AG, Goodrich JK, Gordon JI, et al. QIIME allows analysis of high-throughput community sequencing data. *Nat Methods*. 2010;7(5):335–336. doi:10.1038/nmeth.f.303.
47. Robinson MD, McCarthy DJ, Smyth GK. edgeR: a bioconductor package for differential expression analysis of digital gene expression data. *Bioinformatics*. 2010;26(1):139–140. doi:10.1093/bioinformatics/btp616.
48. McCarthy DJ, Chen Y, Smyth GK. Differential expression analysis of multifactor RNA-Seq experiments with respect to biological variation. *Nucleic Acids Res*. 2012;40(10):4288–4297. doi:10.1093/nar/gks042.
49. Benjamini Y, Hochberg Y. Controlling the false discovery rate: A practical and powerful approach to multiple testing. *J R Statist Soc B*. 1995;57:289–300.
50. Borneman J, Triplett EW. Molecular microbial diversity in soils from eastern Amazonia: evidence for unusual

- microorganisms and microbial population shifts associated with deforestation. *Appl Environ Microbiol*. 1997;63(7):2647–2653. doi:10.1128/AEM.63.7.2647-2653.1997.
51. Mills E, Baruch K, Aviv G, Nitzan M, Rosenshine I. Dynamics of the type III secretion system activity of enteropathogenic *Escherichia coli*. *mBio*. 2013;4(4). doi:10.1128/mBio.00303-13.
 52. Mandel M, Higa A. Calcium-dependent bacteriophage DNA infection. *J Mol Biol*. 1970;53(1):159–162. doi:10.1016/0022-2836(70)90051-3.
 53. Martinez-Medina M, Aldeguer X, Lopez-Siles M, Gonzalez-Huix F, Lopez-Oliu C, Dahbi G, Blanco JE, Blanco J, Garcia-Gil LJ, Darfeuille-Michaud A. Molecular diversity of *Escherichia coli* in the human gut: new ecological evidence supporting the role of adherent-invasive *E. coli* (AIEC) in Crohn's disease. *Inflamm Bowel Dis*. 2009;15(6):872–882. doi:10.1002/ibd.20860.
 54. Baumgart M, Dogan B, Rishniw M, Weitzman G, Bosworth B, Yantiss R, Orsi RH, Wiedmann M, McDonough P, Kim SG, et al. Culture independent analysis of ileal mucosa reveals a selective increase in invasive *Escherichia coli* of novel phylogeny relative to depletion of Clostridiales in Crohn's disease involving the ileum. *Isme J*. 2007;1(5):403–418. doi:10.1038/ismej.2007.52.
 55. Kasper SH, Spalinger MR, Leonardi I, Gerstgrasser A, Raselli T, Gottier C, Atrott K, Frey-Wagner I, Fischbeck-Terhalle A, Rogler G, et al. Deficiency of protein tyrosine phosphatase non-receptor type 2 in intestinal epithelial Cells has no appreciable impact on dextran sulphate sodium colitis severity but promotes wound healing. *Digestion*. 2016;93(4):249–259. doi:10.1159/000445289.
 56. Becker C, Fantini MC, Neurath MF. High resolution colonoscopy in live mice. *Nat Protoc*. 2006;1(6):2900–2904. doi:10.1038/nprot.2006.446.
 57. Friedman DJ, Kunzli BM, Rahim YI, Sevigny J, Berberat PO, Enyoji K, Csizmadia E, Friess H, Robson SC. CD39 deletion exacerbates experimental murine colitis and human polymorphisms increase susceptibility to inflammatory bowel disease. *Proc Natl Acad Sci USA*. 2009;106(39):16788–16793. doi:10.1073/pnas.0902869106.
 58. Spalinger MR, Kasper S, Gottier C, Lang S, Atrott K, Vavricka SR, Scharl S, Raselli T, Frey-Wagner I, Gutte PM, et al. NLRP3 tyrosine phosphorylation is controlled by protein tyrosine phosphatase PTPN22. *J Clin Invest*. 2016;126(5):1783–1800. doi:10.1172/JCI83669.
 59. Tsai PY, Zhang B, He WQ, Zha JM, Odenwald MA, Singh G, Tamura A, Shen L, Sailer A, Yeruva S, et al. IL-22 upregulates epithelial claudin-2 to drive diarrhea and enteric pathogen clearance. *Cell Host Microbe*. 2017;21(6):671–681. doi:10.1016/j.chom.2017.05.009.
 60. Edelblum KL, Sharon G, Singh G, Odenwald MA, Sailer A, Cao S, Ravens S, Thomsen I, El Bissati K, McLeod R, et al. The microbiome activates CD4 T-cell-mediated immunity to compensate for increased intestinal permeability. *Cell Mol Gastroenterol Hepatol*. 2017;4(2):285–297. doi:10.1016/j.jcmgh.2017.06.001.
 61. Bankevich A, Nurk S, Antipov D, Gurevich AA, Dvorkin M, Kulikov AS, Lesin VM, Nikolenko SI, Pham S, Prjibelski AD, et al. SPAdes: a new genome assembly algorithm and its applications to single-cell sequencing. *J Comput Biol*. 2012;19(5):455–477. doi:10.1089/cmb.2012.0021.
 62. Seemann T. Prokka: rapid prokaryotic genome annotation. *Bioinformatics*. 2014;30(14):2068–2069. doi:10.1093/bioinformatics/btu153.
 63. Smith TF, Waterman MS. Identification of common molecular subsequences. *J Mol Biol*. 1981;147(1):195–197. doi:10.1016/0022-2836(81)90087-5.
 64. Madeira F, Park YM, Lee J, Buso N, Gur T, Madhusoodanan N, Basutkar P, Tivey ARN, Potter SC, Finn RD, et al. The EMBL-EBI search and sequence analysis tools APIs in 2019. *Nucleic Acids Res*. 2019;47(W1):W636–W641. doi:10.1093/nar/gkz268.
 65. Curran-Everett D. Multiple comparisons: philosophies and illustrations. *Am J Physiol Regul Integr Comp Physiol*. 2000;279(1):R1–R8. doi:10.1152/ajpregu.2000.279.1.R1.
 66. Marchesi JR. Human distal gut microbiome. *Environ Microbiol*. 2011;13(12):3088–3102. doi:10.1111/j.1462-2920.2011.02574.x.
 67. Camprubi-Font C, Lopez-Siles M, Ferrer-Guixeras M, Niubo-Carulla L, Abella-Ametller C, Garcia-Gil LJ, Martinez-Medina M. Comparative genomics reveals new single-nucleotide polymorphisms that can assist in identification of adherent-invasive *Escherichia coli*. *Sci Rep*. 2018;8(1):2695. doi:10.1038/s41598-018-20843-x.
 68. Martinez-Medina M, Mora A, Blanco M, Lopez C, Alonso MP, Bonacorsi S, Nicolas-Chanoine MH, Darfeuille-Michaud A, Garcia-Gil J, Blanco J. Similarity and divergence among adherent-invasive *Escherichia coli* and extraintestinal pathogenic *E. coli* strains. *J Clin Microbiol*. 2009;47(12):3968–3979. doi:10.1128/JCM.01484-09.
 69. Zhang HJ, Xu B, Wang H, Xu B, Wang GD, Jiang MZ, Lei C, Ding ML, Yu PF, Nie YZ, et al. IL-17 is a protection effector against the adherent-invasive *Escherichia coli* in murine colitis. *Mol Immunol*. 2018;93:166–172. doi:10.1016/j.molimm.2017.11.020.
 70. Barnich N, Carvalho FA, Glasser AL, Darcha C, Jantschkeff P, Allez M, Peeters H, Bommelaer G, Desreumaux P, Colombel JF, et al. CEACAM6 acts as a receptor for adherent-invasive *E. coli*, supporting ileal mucosa colonization in Crohn disease. *J Clin Invest*. 2007;117(6):1566–1574. doi:10.1172/JCI30504.
 71. Boisen N, Scheutz F, Rasko DA, Redman JC, Persson S, Simon J, Kotloff KL, Levine MM, Sow S, Tamboura B, et al. Genomic characterization of enteroaggregative *Escherichia coli* from children in Mali. *J Infect Dis*. 2012;205(3):431–444. doi:10.1093/infdis/jir757.

72. Verma R, Rojas TCG, Maluta RP, Leite JL, da Silva LPM, Nakazato G, Dias da Silveira W, McCormick BA. Fimbria-encoding gene *yadC* has a pleiotropic effect on several biological characteristics and plays a role in avian pathogenic *Escherichia coli* pathogenicity. *Infect Immun*. 2016;84(1):187–193. doi:10.1128/IAI.01138-15.
73. Nash JH, Villegas A, Kropinski AM, Aguilar-Valenzuela R, Konczyk P, Mascarenhas M, Ziebell K, Torres AG, Karmali MA, Coombes BK. Genome sequence of adherent-invasive *Escherichia coli* and comparative genomic analysis with other *E. coli* pathotypes. *BMC Genomics*. 2010;11:667. doi:10.1186/1471-2164-11-667.
74. Ravan H, Amandadi M. Analysis of *yeh* fimbrial gene cluster in *Escherichia coli* O157: h7 in order to find a genetic marker for this serotype. *Curr Microbiol*. 2015;71(2):274–282. doi:10.1007/s00284-015-0842-6.
75. Spurbeck RR, Stapleton AE, Johnson JR, Walk ST, Hooton TM, Mobley HLT. Fimbrial profiles predict virulence of uropathogenic *Escherichia coli* strains: contribution of *ygi* and *yad* fimbriae. *Infect Immun*. 2011;79(12):4753–4763. doi:10.1128/IAI.05621-11.
76. Allen KJ, Lepp D, McKellar RC, Griffiths MW. Examination of stress and virulence gene expression in *Escherichia coli* O157: h7 using targeted microarray analysis. *Foodborne Pathog Dis*. 2008;5(4):437–447. doi:10.1089/fpd.2008.0100.
77. Gibold L, Garenaux E, Dalmaso G, Gallucci C, Cia D, Mottet-Auselo B, Fais T, Darfeuille-Michaud A, Nguyen HTT, Barnich N, et al. The Vat-AIEC protease promotes crossing of the intestinal mucus layer by Crohn's disease-associated *Escherichia coli*. *Cell Microbiol*. 2016;18(5):617–631. doi:10.1111/cmi.12539.
78. Mattar R, Marques SB, Monteiro M, Dos Santos AF, Iriya K, Carrilho FJ. *Helicobacter pylori* *cag* pathogenicity island genes: clinical relevance for peptic ulcer disease development in Brazil. *J Med Microbiol*. 2007;56 (Pt 1):9–14. doi:10.1099/jmm.0.46824-0.
79. Claret L, Miquel S, Vieille N, Ryjenkov DA, Gomelsky M, Darfeuille-Michaud A. The flagellar sigma factor FliA regulates adhesion and invasion of Crohn disease-associated *Escherichia coli* via a cyclic dimeric GMP-dependent pathway. *J Biol Chem*. 2007;282 (46):33275–33283. doi:10.1074/jbc.M702800200.
80. O'Brien CL, Bringer MA, Holt KE, Gordon DM, Dubois AL, Barnich N, Darfeuille-Michaud A, Pavli P. Comparative genomics of Crohn's disease-associated adherent-invasive *Escherichia coli*. *Gut*. 2017;66 (8):1382–1389. doi:10.1136/gutjnl-2015-311059.
81. Lee JG, Han DS, Jo SV, Lee AR, Park CH, Eun CS, Lee Y. Characteristics and pathogenic role of adherent-invasive *Escherichia coli* in inflammatory bowel disease: potential impact on clinical outcomes. *PLoS One*. 2019;14(4):e0216165. doi:10.1371/journal.pone.0216165.
82. Kotlowski R, Bernstein CN, Sepehri S, Krause DO. High prevalence of *Escherichia coli* belonging to the B2+D phylogenetic group in inflammatory bowel disease. *Gut*. 2007;56(5):669–675. doi:10.1136/gut.2006.099796.
83. Hausmann M, Rechsteiner T, Caj M, Benden C, Fried M, Boehler A, Rogler G. A new heterotopic transplant animal model of intestinal fibrosis. *Inflamm Bowel Dis*. 2013;19(11):2302–2314. doi:10.1097/MIB.0b013e3182a6a0f3.
84. Mirsepasi-Lauridsen HC, Vallance BA, Krogfelt KA, Petersen AM. *Escherichia coli* pathobionts associated with inflammatory bowel disease. *Clin Microbiol Rev*. 2019;32:2. doi:10.1128/CMR.00060-18.
85. Small CL, Xing L, McPhee JB, Law HT, Coombes BK. Acute infectious gastroenteritis potentiates a Crohn's disease pathobiont to fuel ongoing inflammation in the post-infectious period. *PLoS Pathog*. 2016;12(10):e1005907. doi:10.1371/journal.ppat.1005907.